ENSO-Unrelated Variability in Indo–Northwest Pacific Climate: Regional Coupled Ocean–Atmospheric Feedback

CHUAN-YANG WANG

Physical Oceanography Laboratory/Qingdao Collaborative Innovation Center of Marine Science and Technology, Ocean University of China, and Qingdao National Laboratory for Marine Science and Technology, Qingdao, China

SHANG-PING XIE

Scripps Institution of Oceanography, University of California, San Diego, La Jolla, California

YU KOSAKA

Research Center for Advanced Science and Technology, The University of Tokyo, Tokyo, Japan

(Manuscript received 9 June 2019, in final form 18 February 2020)

ABSTRACT

Regional ocean–atmospheric interactions in the summer tropical Indo–northwest Pacific region are investigated using a tropical Pacific Ocean–global atmosphere pacemaker experiment with a coupled ocean–atmospheric model (cPOGA) and a parallel atmosphere model simulation (aPOGA) forced with sea surface temperature (SST) variations from cPOGA. Whereas the ensemble mean features pronounced influences of El Niño–Southern Oscillation (ENSO), the ensemble spread represents internal variability unrelated to ENSO. By comparing the aPOGA and cPOGA, this study examines the effect of the ocean–atmosphere coupling on the ENSO-unrelated variability. In boreal summer, ocean–atmosphere coupling induces local positive feedback to enhance the variance and persistence of the sea level pressure and rainfall variability over the northwest Pacific and likewise induces local negative feedback to suppress the variance and persistence of the sea level pressure and rainfall variability over the north Indian Ocean. Anomalous surface heat fluxes induced by internal atmosphere variability cause SST to change, and SST anomalies feed back onto the atmosphere through atmospheric convection. The local feedback is sensitive to the background winds: positive under the mean easterlies and negative under the mean westerlies. In addition, north Indian Ocean SST anomalies reinforce the low-level anomalous circulation over the northwest Pacific through atmospheric Kelvin waves. This interbasin interaction, along with the local feedback, strengthens both the variance and persistence of atmospheric variability over the northwest Pacific. The response of the regional Indo–northwest Pacific mode to ENSO and influences on the Asian summer monsoon are discussed.

1. Introduction

In summer, interannual variability in the Indo–northwestern Pacific (Indo-NWP) region features a recurrent pattern with a low-level anomalous anticyclone (AAC). The AAC is closely related to El Niño–Southern Oscillation (ENSO) (e.g., Wang et al. 2000, 2003; Lu 2001). ENSO typically begins to develop in summer [June–August (JJA)], peaks in winter (December–February), and decays rapidly in the following spring (March–May). Seasons in this paper refer to those in the Northern Hemisphere. The AAC often emerges in the El Niño winter and persists through the following summer (Zhang et al. 1996; Wang et al. 2000).

While recent studies show that the abrupt onset of the AAC is possibly tied to nonlinear interactions between the annual cycle and ENSO (Stuecker et al. 2013, 2015; Xie and Zhou 2017), ocean–atmosphere coupling plays key roles in helping the AAC persist into the following summer (e.g., Wang et al. 2000; Wu and Yeh 2008, 2010; Kosaka et al. 2013; Xie et al. 2016). Wang et al. (2000) suggest that wind–evaporation–SST (WES) feedback over the NWP is important for the formation and persistence of the AAC in winter and spring. The anomalous northeasterlies on the southeast flank of the AAC increase the northeast background trades and cool the

Corresponding author: Shang-Ping Xie, sxie@ucsd.edu

DOI: 10.1175/JCLI-D-19-0426.1

ocean with increased evaporation while the cold SST anomalies in turn suppress local convection and support the AAC via an atmospheric Rossby wave response (Wang et al. 2000). This WES feedback requires easterly background winds, which retreat and weaken over the NWP in summer. The SST anomalies over the tropical Indian Ocean (IO) also contribute to the development of the summer AAC (Ohba and Ueda 2006; Xie et al. 2009; Wu and Yeh 2010; Hu et al. 2019). Anomalously warm SSTs in the tropical IO excite a Matsuno–Gill pattern (Matsuno 1966; Gill 1980) with an eastward-propagating Kelvin wave. The Kelvin wave supports the AAC by inducing low-level Ekman divergence due to the friction (Terao and Kubota 2005; Xie et al. 2009). Recent studies show that the AAC can feed back to north IO (NIO) SST through the anomalous easterlies by weakening the background southwest monsoon and suppressing local evaporation (Kosaka et al. 2013; Xie et al. 2016). Therefore, the AAC and warm NIO form an interbasin positive feedback (Kosaka et al. 2013). The Indo–western Pacific Ocean capacitor (IPOC) mode refers to the above coherent coupled anomalies over the tropical IO and NWP in the post–El Niño summer (Fig. 1; Xie et al. 2016, Xie and Zhou 2017).

Whereas the IPOC is closely tied to ENSO in observations, recent model studies show that regional positive feedbacks can sustain the IPOC without ENSO forcing (e.g., Kosaka et al. 2013; Wang et al. 2018). Indeed, by linearly removing ENSO in observations (Wang et al. 2018), or in partially coupled models without ENSO forcing (Kosaka et al. 2013), an ENSO-unrelated IPOC mode emerges, resembling the original IPOC and supported by regional coupling processes. Such ENSO-unrelated, internal variability makes up a large portion of the interannual variability (Wang et al. 2018) and can causes uncertainties in Indo-NWP climate prediction (Ma et al. 2017). The complex nature of Indo-NWP summer climate variability and its potential social impact call for a better understanding of the internal variabilities, specifically, what roles does the ocean–atmosphere coupling play in supporting the ENSO-unrelated IPOC and how it is different from the ENSO-forced IPOC? Since the Indo-NWP region is strongly influenced by monsoons, the regional ocean–atmosphere interactions may show strong seasonality.

This study examines regional ocean–atmospheric coupled processes in the Indo-NWP region by comparing a pair of atmosphere-only and coupled Pacific Ocean–global atmosphere (POGA) ensembles, each with nine members. The POGA experiment is a useful tool to study global and regional climate variability (e.g., Kosaka et al. 2013; Kosaka and Xie 2013, 2016; Yang et al. 2015; Zhang et al. 2018). In the coupled POGA (cPOGA), SST

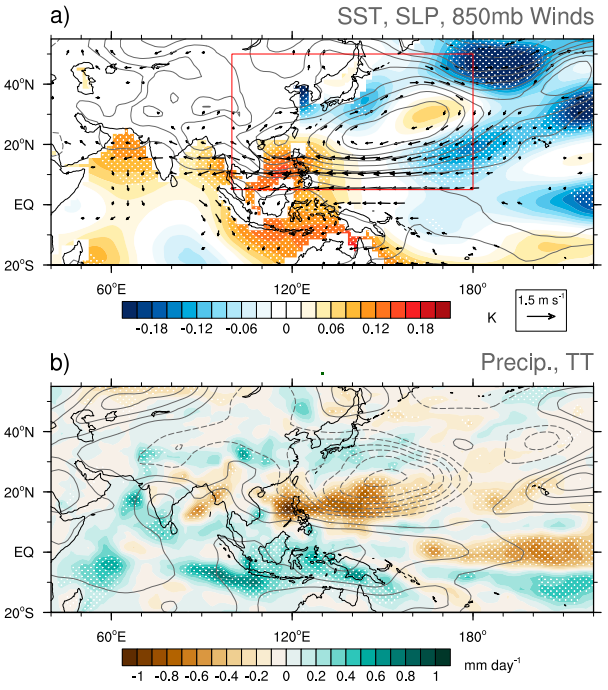

FIG. 1. IPOC mode as represented by observed (1948–2016) JJA anomalies of (a) SST (shading), SLP (contours, every 0.1 hPa with the zero contour omitted), and 850-hPa winds (arrows; only >95% confidence level are shown) (b) precipitation (shading) and normalized tropospheric temperature averaged between 850 and 300 hPa (contours; every 0.1 with the zero contour omitted) associated with the principal component of the leading empirical orthogonal function mode (explaining 40% of the total variance) of the NWP SLP [Red box in (a): 10°–50°N, 100°E–180°]. SST and precipitation anomalies at >95% confidence level are stippled, based on the *t* test. SST and atmosphere variables are from Extended Reconstructed Sea Surface Temperature v4 (ERSST v4, Huang et al. 2015) and National Centers for Environmental Prediction–National Center for Atmospheric Research reanalysis (Kalnay et al. 1996), respectively.

anomalies in the tropical eastern Pacific are restored toward monthly observations. The ensemble mean SST from cPOGA is used to force the atmosphere-only POGA (aPOGA). The ensemble spread represents the ENSO-unrelated coupled internal variability in the cPOGA and the ENSO-unrelated atmospheric internal variability in the aPOGA. We start by analyzing the persistence and interannual variance of the summer atmospheric variabilities in the Indo-NWP region. The sea level pressure (SLP) and precipitation anomalies over the NWP show enhanced interannual variance and are more persistent in the cPOGA than in the aPOGA. The AAC cools the NWP under the northeasterly background winds and the local SST effect in turn enhances the AAC. Conversely, SLP and precipitation anomalies over the NIO show suppressed interannual variance and are less persistent in the cPOGA than in

the aPOGA. The AAC warms the NIO under the southwesterly background winds and the local SST effect in turn suppresses the AAC. The warm IO also induces an interbasin positive feedback in support of the AAC.The seasonal evolution of Indo-NWP climate variability indicates that the local feedback is tied to the background winds, positive under the mean easterlies and negative under the westerlies. This study shows that ocean–atmosphere coupling plays key roles in modulating the interannual variability of the atmospheric anomalies, and it can potentially enhance the predictability of the summer Indo–western Pacific climate variability.

The rest of the paper is organized as follows. Section 2 describes the data and methods. Section 3 examines the variance and persistence of summer Indo-NWP climate variability. Section 4 investigates dominant ocean–atmosphere feedbacks and the favorable conditions in the Indo-NWP region in summer. Section 5 discusses the seasonal evolution of the ocean–atmosphere coupled processes. Section 6 is a summary.

2. Data and methods

We analyze the output of the POGA experiments [see Kosaka et al. (2013) for a detailed description of the experiment]. The coupled version (cPOGA) is based on the Geophysical Fluid Dynamics Laboratory coupled model, version 2.1 (CM2.1, Delworth et al. 2006), consisting of nine members. Each member starts with different initial conditions but shares the same radiative forcing. Over the eastern tropical Pacific (15°S–15°N, with a 5° buffer zone, from the date line to the American coast), SST anomalies are restored to follow the observed evolution derived from Hadley Centre Sea Ice and SST, version 1.1 (Rayner et al. 2003), while the ocean and atmosphere are fully coupled elsewhere. The ensemble mean of the monthly cPOGA SST is used globally to force the atmospheric model to form a parallel nine-member aPOGA ensemble. Both experiments have been performed from 1950 to 2010.

We examine the ENSO-unrelated and atmospheric internal variability estimated as the ensemble spread by subtracting the ensemble mean from the raw output. The ensemble spread of the cPOGA represents the ENSO-unrelated coupled variability, as each member is forced by the same external forcing and tropical Pacific SST. The ensemble spread of the aPOGA captures the atmospheric internal variability, equivalent to an AGCM forced by the repeating climatological SST, as every member is forced by the same radiative forcing and global SST. The comparison of the aPOGA and cPOGA allows us to study how the ocean and atmosphere interact in the Indo-NWP region without ENSO forcing.

All variables used in this study are interpolated onto a common $1° \times 1°$ grid. As the ENSO-unrelated IPOC shows strong interannual variability with peak frequencies smaller than 9 years (not shown), we apply an 11-point Lanczos high-pass filter with half-power at 11 years for all the variables at each grid point to remove the decadal variability and long-term trends in both the model and observations. Although Sullivan et al. (2016) show that the central Pacific SST features a spectral peak at 10–11 yr, which may affect the NWP AAC (Fan et al. 2013), our comparison between 9- and 11-yr high-pass filters yields similar results. The first 10 years are discarded as the spinup. To get better statistical results, the same variables among the nine-member intermember spread are concatenated temporally to form a composed variable of 459-yr-long time series in both aPOGA and cPOGA. All analyses in this study, unless otherwise specified, are done with the concatenated series.

3. Summer SLP and precipitation variability

We start by comparing the interannual variance of the JJA SLP and precipitation between the aPOGA and cPOGA (Fig. 2). The SLP variance increases with latitude with zonal maxima over the NIO and NWP along 20°N. Despite the broad resemblance between the aPOGA and cPOGA, the two experiments show discrepancies in the spatial distribution of the SLP variance, especially over the NIO, NWP, and southern tropical IO (Figs. 2c,d). Because the ENSO variability is suppressed in the ensemble spread, the difference between cPOGA and aPOGA is likely due to regional ocean–atmosphere coupling. The cPOGA shows the increased variance over the equatorial Indian Ocean and NWP and the decreased variance over the NIO relative to the aPOGA, suggesting different types of coupling processes among those regions. The increased or decreased variance in cPOGA may suggest a local positive or negative ocean–atmosphere feedback, respectively. The enhanced variance over the equatorial IO is likely due to the Indian Ocean dipole mode, as has been documented in previous studies (e.g., Yang et al. 2015). In this study, we only focus on the NIO and NWP regions.

The summer precipitation shows high interannual variance over the intertropical convergence zone, South Pacific convergence zone, and the warm pool region in both aPOGA and cPOGA (Figs. 2a,b), similar to the climatological rainfall distribution (not shown). Over the NIO, precipitation variance is suppressed in the cPOGA compared to the aPOGA, consistent with the

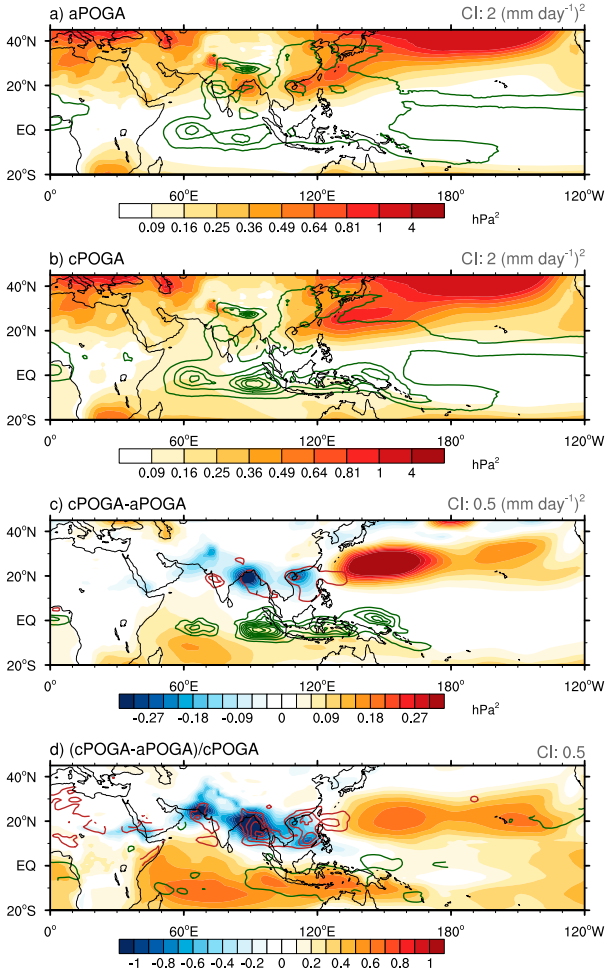

FIG. 2. Interannual variance of JJA SLP (shading) and precipitation (contours, with intervals on the top right of the panels) in (a) aPOGA and (b) cPOGA, and their (c) difference and (d) fractional difference, shown as the difference divided by the cPOGA variance. Positive and negative are in green and dark red contours, respectively, with the zero contour omitted. Contours in (a) and (b) start with 1 (mm day^{-1})^2.

SLP pattern. Similar rainfall variance differences in the NIO are documented by Zhou et al. (2018), who compare the variance between a CGCM simulation and an Atmospheric Model Intercomparison Project (AMIP)-like simulation forced by CGCM SST variability. They argue that the overestimated precipitation variability in the AMIP-like simulation is due to the lack of local negative ocean feedbacks despite identical monthly SST forcing in two experiments. Climatological precipitation is slightly stronger (5%–10%; figures not shown) in the cPOGA than the aPOGA over the NWP and South China Sea (SCS). The difference in the precipitation climatology is much smaller than the difference in the interannual variance (typically >50%; Fig. 2d), suggesting the importance of ocean–atmosphere coupling for interannual variability. Monthly averaged SLP and precipitation variance distributions are qualitatively consistent with the seasonal mean but with larger amplitudes.

Ocean–atmosphere coupling alters not only SLP and precipitation variance but also their temporal persistence. Figure 3 shows local pointwise lag correlations with July SLP and precipitation in the cPOGA. SLP shows significant lagged correlations over the NWP and equatorial IO, even at 2-month lead/lag. Over the NIO, the SLP and precipitation anomalies show weak and even negative lag correlations, suggesting weak persistence and negative local feedback. The autocorrelation pattern broadly agrees with the variance difference discussed above, with high and low correlations collocated with enhanced and suppressed variability, respectively, over the NWP and equatorial IO in the coupled model. The same analysis in the aPOGA shows insignificantly small correlations over the entire Indo–northwest Pacific region even at 1-month lead/lag, because of the transient nature of atmospheric internal variability (not shown). The contrast in persistence and variance between the NIO and NWP suggests different types of ocean–atmosphere coupling in those regions. We will discuss the possible ocean–atmosphere processes in the following sections.

4. Coupling effect in summer

Wang et al. (2018) uses an area-averaged SLP index to trace the ENSO-unrelated IPOC variability in observations and the coupled POGA experiment. In this study, we employ the same method, but further extend to both aPOGA and cPOGA to explore the roles of coupled dynamics in the ENSO-unrelated IPOC. We first define an NWP SLP index as the area average of SLP anomalies over the tropical NWP region (10°–30°N, 120°E–180°). With the ENSO-forced variability removed in both aPOGA and cPOGA (section 2), the SLP index represents the non-ENSO variability. The SLP index can reasonably capture the dominant mode of the 850-hPa relative vorticity over the northwestern Pacific (0°–60°N, 100°–160°E), especially in the tropical to subtropical regions (not shown). The SLP index and leading principal component of the relative vorticity correlate at 0.52 and 0.62 for aPOGA and cPOGA, respectively. We choose to study the monthly mean because the internal atmospheric anomalies in the aPOGA usually do not last more than one month. Analysis based on seasonal mean yields qualitatively similar results but with much reduced amplitude in the aPOGA.

The SLP index in the coupled model has slightly stronger interannual standard deviation (by ~24%) as

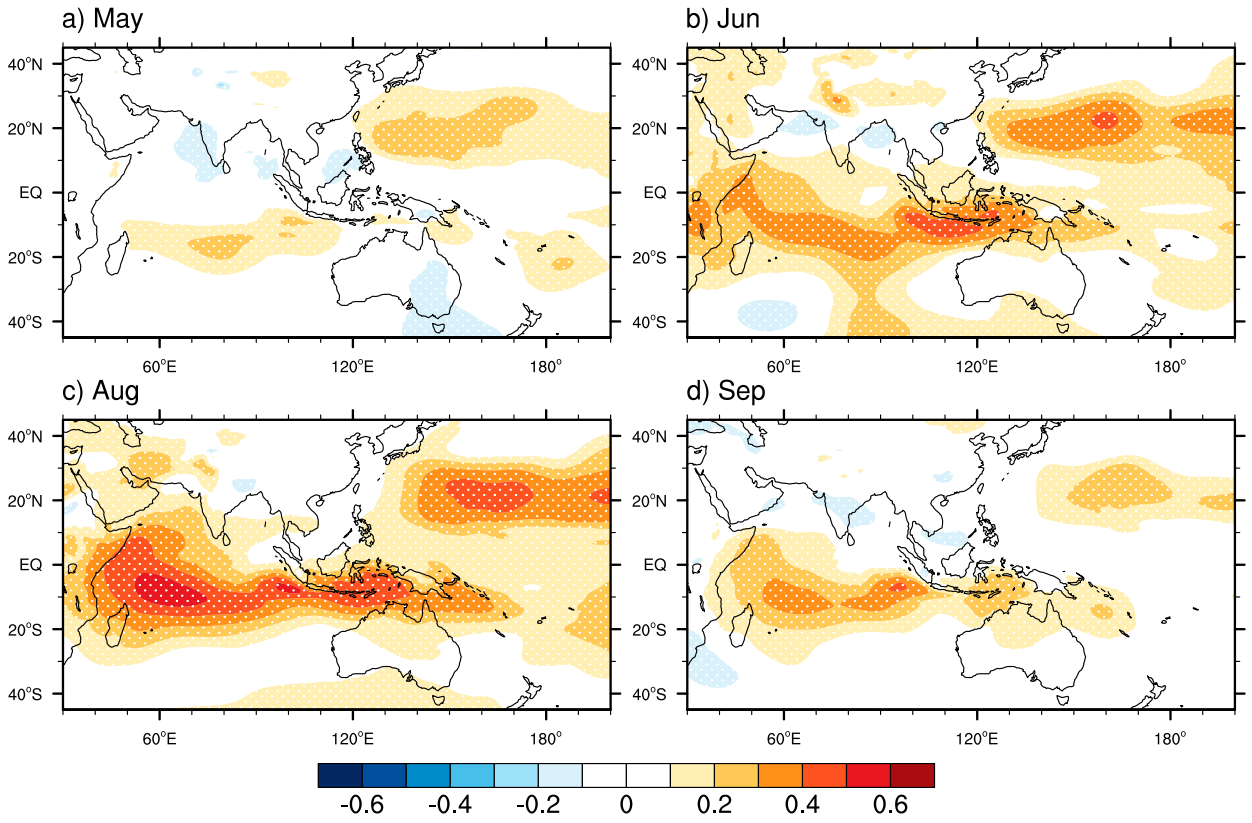

FIG. 3. Pointwise correlation coefficient of (a) May, (b) June, (c) August, and (d) September SLP with July SLP in cPOGA. Correlation coefficients at >95% confidence level are stippled, based on the *t* test.

discussed above, likely due to ocean–atmosphere coupling. To capture the variance difference induced by the coupling processes, we compute the regression coefficients of the SLP, 850-hPa winds, precipitation, normalized troposphere temperature, and SST (only in the coupled model) against the NWP SLP index (Fig. 4). The ENSO-unrelated IPOC mode shows a strong resemblance to the observed counterpart except for the SST anomalies over the tropical southwestern IO (Figs. 1, 4), consistent with previous findings (Kosaka et al. 2013; Wang et al. 2018). Both aPOGA and cPOGA show positive SLP anomalies over the NWP, accompanied with an AAC and suppressed precipitation. One major difference between the aPOGA and cPOGA is the westward extension of the SLP and circulation patterns. Positive SLP anomalies extend farther westward over the Arabian Sea in the aPOGA, while in the cPOGA, the SLP anomalies diminish quickly over the Bay of Bengal (BOB) and to the west. Similar patterns can also be found in the precipitation anomalies (Figs. 4b,d). Significant negative precipitation anomalies reside in the SCS and BOB in the aPOGA but are weak in the coupled model. The weak SLP and precipitation anomalies over the NIO in the cPOGA suggests that the local ocean–atmosphere coupling induces negative feedback. In the BOB and SCS, positive SST anomalies, opposing the AAC effect, reduce local precipitation anomalies below 95% significance level. On the other hand, the positive SST anomalies in the IO excite a Matsuno–Gill pattern (Fig. 4b) over the tropical IO and "Maritime Continent" that reinforces the AAC over the NWP via the Kelvin wave–induced divergence mechanism (Xie et al. 2009). The anomalous easterlies on the south flank of the AAC in turn warm the NIO SST by reducing the background westerly monsoon wind. The response in tropospheric temperature is insignificant in the aPOGA because of the lack of SST forcing (Fig. 4d). Precipitation anomalies associated with the AAC over the NWP are mostly over the ocean but are notably large over the Maritime Continent, India, and eastern China. The ENSO-unrelated IPOC mode can potentially contribute to the summer rainfall variability over these regions.

To understand the atmospheric impact on the ocean, we compare the SST tendency and anomalous heat fluxes in July in the cPOGA (Fig. 5). A strong positive SST tendency is found in the SCS and western Pacific while moderate warming exists in the BOB and Arabian Sea. Largely contributed by anomalous shortwave and

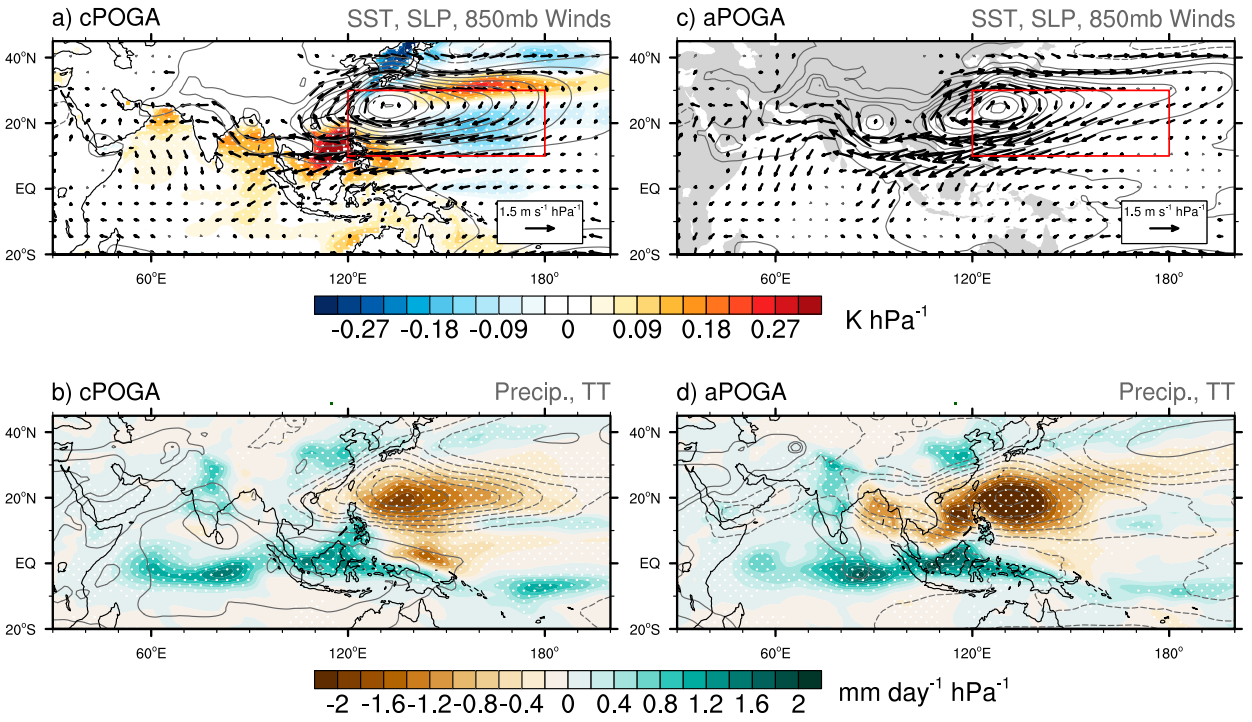

FIG. 4. July anomalies of (a),(c) SST (shading; K hPa^{-1}), SLP (contours, every 0.1 hPa hPa^{-1} with the zero contour omitted), and 850-hPa winds (arrows) and (b),(d) precipitation (shading) and normalized tropospheric temperature averaged between 850 and 300 hPa (contours, every 0.1 hPa^{-1} with the zero contour omitted) associated with July NWP SLP index in (left) cPOGA and (right) aPOGA. SST and precipitation regressions at >95% confidence level are stippled, based on the *t* test. SST regressions in aPOGA [(c)] are equal to zero because SST anomalies in aPOGA are always zero by design (section 2).

latent heat fluxes, net surface heat flux anomalies show good correspondence to the SST tendency, except over the SCS and part of the Arabian Sea where ocean dynamics seems also important (Wang et al. 2002; Xie et al. 2003; Izumo et al. 2008). In the tropical NWP, suppressed convection increases the downward shortwave radiation while the latent heat flux resembles the spatial distribution of the anomalous easterlies (Fig. 4a). The SST tendency and net surface heat flux shows positive anomalies in the BOB but with smaller magnitude than in the NWP. In fact, the SST shows a strong positive tendency in June due to the anomalous easterlies in the NIO and SCS region (not shown).

We further decompose the latent heat fluxes into the flux induced by anomalous atmospheric forcing (AtF; Fig. 5f) and a Newtonian cooling effect related to SST-induced evaporation (not shown) following Du et al. (2009). The warm SST in the NIO (Fig. 4a) induces a strong Newtonian cooling, which is compensated by the warming effect due to the wind speed reduction by anomalous easterlies. The net effect of these two processes helps the positive SST anomalies to persist. Over the NWP sector, the latent heat flux is mainly contributed by the AtF term, suggesting the key role of atmospheric variability (e.g., wind).

We then estimate the SST effect on the atmosphere. SLP variability over the subtropical NWP increases due to ocean–atmosphere coupling (Fig. 2). Ocean–atmospheric variability in the coupled model comprises atmospheric internal variability and the coupled feedback (cFB):

$$R_c\sigma(\mathrm{SLP}_c') = R_a\sigma(\mathrm{SLP}_a') + \mathrm{cFB},$$

where R is the regression coefficient against the NWP SLP index, $\sigma(\mathrm{SLP}')$ denotes the standard deviation of the SLP index, and subscripts a and c denote the results from coupled and atmospheric models, respectively.

Figure 6 shows the coupled feedback:

$$\mathrm{cFB} \equiv R_c\sigma(\mathrm{SLP}_c') - R_a\sigma(\mathrm{SLP}_a').$$

Shading in Fig. 6a shows the SST anomalies associated with NWP SLP variability in the cPOGA. Anomalous high pressure deviations are accompanied by AAC over the NWP and anomalous cool SST on the southeast flank, and anomalous low pressure deviations are accompanied by an anomalous cyclone over the SCS and BOB and anomalous warm SST on the southeast flank, all of which suggest a Rossby wave response to convective heating. Positive precipitation deviations

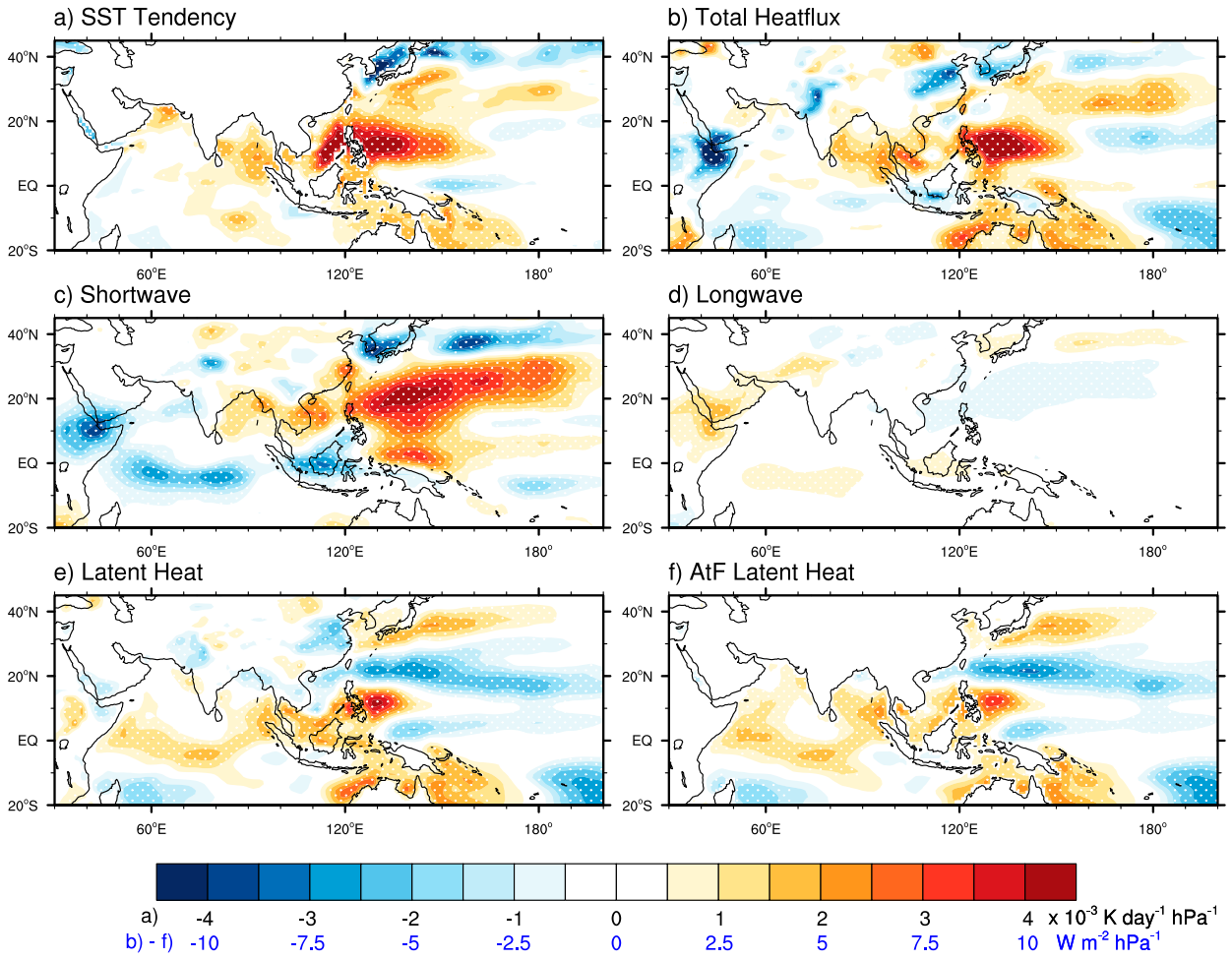

FIG. 5. July anomalies of (a) SST tendency, (b) total surface heat flux, (c) shortwave radiation, (d) longwave radiation, (e) total latent heat flux, and (f) latent heat flux induced by anomalous atmospheric forcings, regressed against the July NWP SLP index in the cPOGA. Regression coefficients at >95% confidence level are stippled, based on the *t* test.

over the BOB and SCS and negative deviations over the tropical NWP (Fig. 6b) are consistent with the SST anomaly distribution. This suggests that the atmospheric variability differences between cPOGA and aPOGA can be attributed to the local SST forcing. The precipitation deviations induced by anomalous SST are of opposite signs to the atmospheric internal variability over the BOB and SCS (Fig. 6b vs Fig. 4d), while reinforcing that over the NWP. This suggests that when coupled, SST-induced local atmosphere response enhances atmosphere variability over the NWP but suppresses the atmospheric internal variability over the NIO. In the Indo-NWP region, the sign of the local WES feedback is determined by the background wind, positive under the mean easterlies while negative under the mean westerlies. Apart from the local feedbacks, positive SST anomalies over BOB and SCS drive a prominent Matsuno–Gill pattern in tropospheric temperature and an interbasin feedback on the NWP AAC (Fig. 6b) as discussed above. The spatial distribution, persistence and variance of the coupled ocean–atmospheric variability in the Indo-NWP region are modulated coordinately by both local and interbasin feedback processes.

To examine the evolution of the ENSO-unrelated IPOC, we compute the lag correlations of SSTs in different basins with the NWP SLP index (Fig. 7a). As discussed above, the NWP SLP shows persistence only in the cPOGA. The SSTs in the NWP are negatively correlated with July NWP SLP in spring and early summer, reaching maximum in July, decreasing afterward, and becoming insignificant in September. The SST correlation in the NIO and SCS, on the other hand, is weak before July but stays positive in July and August. Over the NWP, SST leads SLP, suggesting that the ocean has a strong impact on the atmosphere. Likewise, the lagged cross correlations

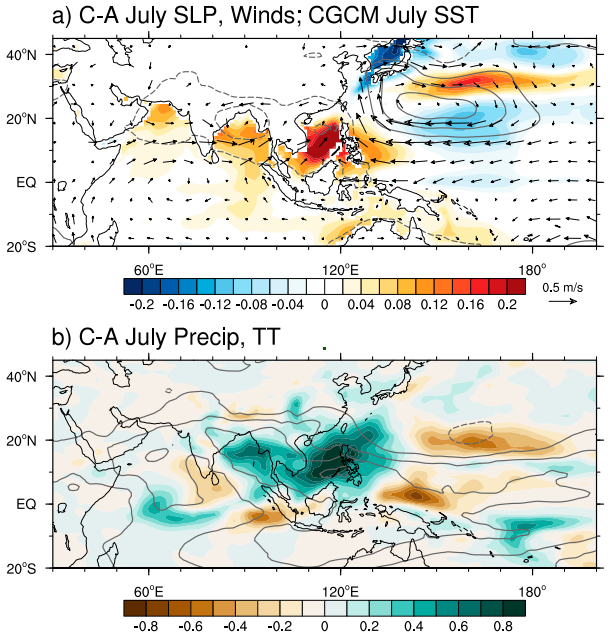

FIG. 6. Coupled feedbacks (cFB) of July (a) SLP (contours, every 1 hPa with zero line omitted) and 850-hPa winds (arrows) and (b) normalized tropospheric temperature averaged between 850 and 300 hPa (contours, every 0.1 with zero line omitted) and precipitation (shading; mm day^{-1}) based on normalized July NWP SLP index. The shading in (a) shows the SST regression anomalies (K) against normalized July NWP SLP index in cPOGA.

indicate that the NIO SST is influenced by the atmosphere (Frankignoul and Hasselmann 1977). The POGA may overestimate the correlations between NWP SST and NWP SLP in July due to the overestimated mean easterlies compared to observations, but similar evolution is found in preceding months (May and June; not shown).

We have done a parallel analysis on the July SLP variability over the BOB and SCS (Fig. 7b). There, the autocorrelation coefficient in the cPOGA is slightly smaller at 1-month lag than in the aPOGA, in sharp contrast to the persistent SLP anomalies over the NWP (Fig. 7a). The SLP correlation between the NWP and BOB–SCS is significant both concurrently and when NWP lags BOB–SCS for 1 month. Furthermore, NIO SST correlations are high with SLP when SST lags SLP by one month. These correlations suggest an interbasin positive feedback between the NIO and NWP. As discussed earlier, increased solar radiation and suppressed evaporation accompanied with the AAC induces surface warming in the NIO, and increased SST excites the Matsuno–Gill pattern and helps in sustaining the NWP AAC.

5. Seasonal evolution of the Indo-NWP atmosphere anomalies

As discussed above, the positive and negative feedbacks in the summer Indo-NWP region are determined by the climatological winds of prominent seasonality. In spring, the northeasterlies prevail over the NIO, favorable for the positive WES feedbacks. After the summer monsoon onset, climatological southwesterlies suppress local WES feedback but are essential for the interbasin positive feedback.

In this section, we examine the seasonal evolution of the IPOC mode. Figure 8 shows the lag correlations of the monthly mean Indo–western Pacific SLP, low-level circulation, precipitation, and SST averaged in 5°–25°N

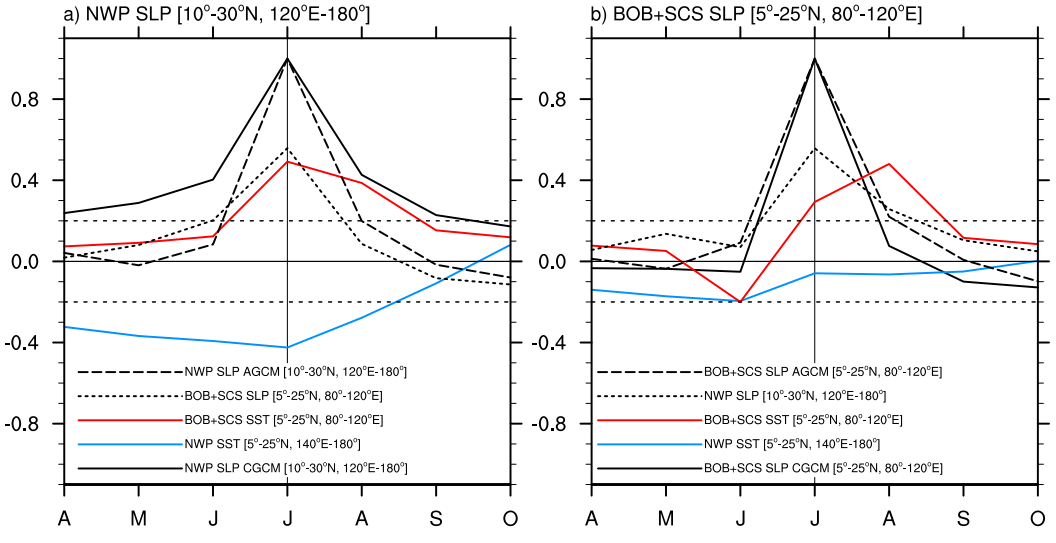

FIG. 7. Cross correlations of SLP and SST in different basins with (a) NWP SLP and (b) BOB and SCS SLP in July. The long dashed curve is based on aPOGA, and the rest are based on cPOGA. Dashed horizontal lines denote ±0.2.

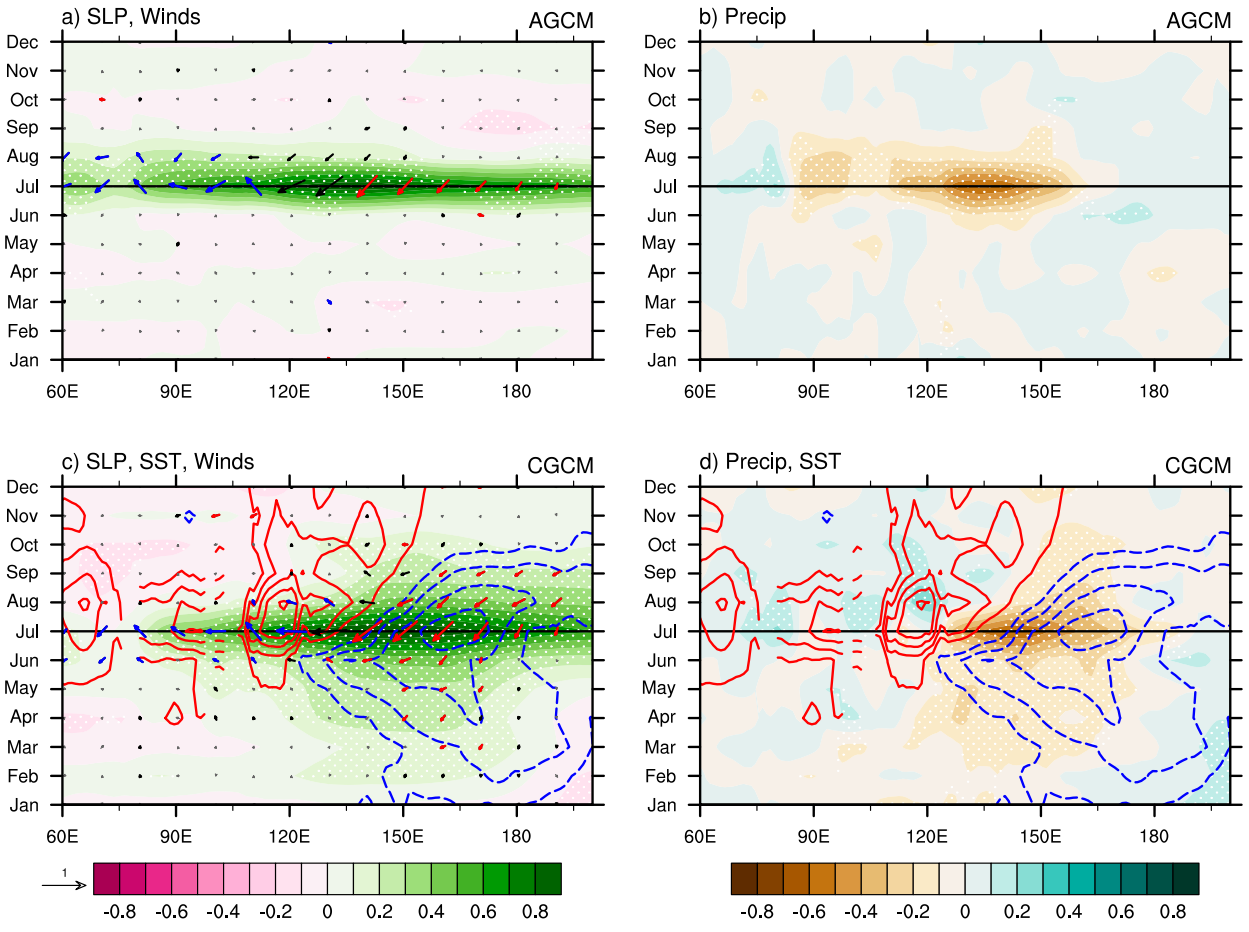

FIG. 8. Seasonal evolution of the ENSO-unrelated IPOC mode represented by the correlations of (a),(c) SLP (shading), 850-hPa winds (arrows), and SST (contours, every 0.1 with zero line omitted) and (b),(d) precipitation (shading) and SST (contours, every 0.1 with zero line omitted) averaged over 5°–25°N with the July NWP SLP index in (top) aPOGA and (bottom) cPOGA. Red or blue contours indicate positive or negative SST anomalies, respectively. Red or blue arrows indicate wind anomalies that strengthen or weaken climatological winds, respectively. Stippling and thick arrows indicate the >95% confidence level for SLP anomalies, and 850-hPa winds, respectively, based on the *t* test.

with the NWP SLP index. An analysis with seasonal means shows qualitatively similar results. In the aPOGA, the SLP, wind, and precipitation anomalies show significant correlations only concurrently because of lack of memory beyond a month. In the coupled model, on the other hand, the NWP SLP shows high correlations throughout the summer with suppressed precipitation and anomalous easterlies over the NWP sector. Negative SST anomalies precede the positive SLP anomalies in the NWP in spring and early summer and retreat eastward after June. Positive SST correlations with the NWP SLP index develop in the NIO and SCS concurrently and expand eastward to the NWP in the late summer and early fall. The evolution of the SST correlations closely follows the retreat of the northeast trades, consistent with previous studies (Xie et al. 2016). The lag correlations of SLP in the mean westerly regime tend to be weak, pointing to a negative local feedback under the background westerlies.

Next, we examine the seasonal evolution of the SLP persistence in the cPOGA ensemble spread. Figure 9a shows the lagged autocorrelation of SLP anomalies over the BOB and SCS with different reference months. The SLP in this region shows weak persistence in summer due to local negative feedback while the SLP persistence is strong in spring when the mean easterlies prevail. The evolution of the SLP persistence is consistent with that of the climatological winds. Figure 10a shows the variance difference between the cPOGA and aPOGA averaged over 5°–25°N in the Indo-NWP region. Similar to the persistence, SLP variance in the cPOGA decreases relative to the aPOGA over the BOB–SCS region during summer when the climatological zonal wind switches from easterly to westerly.

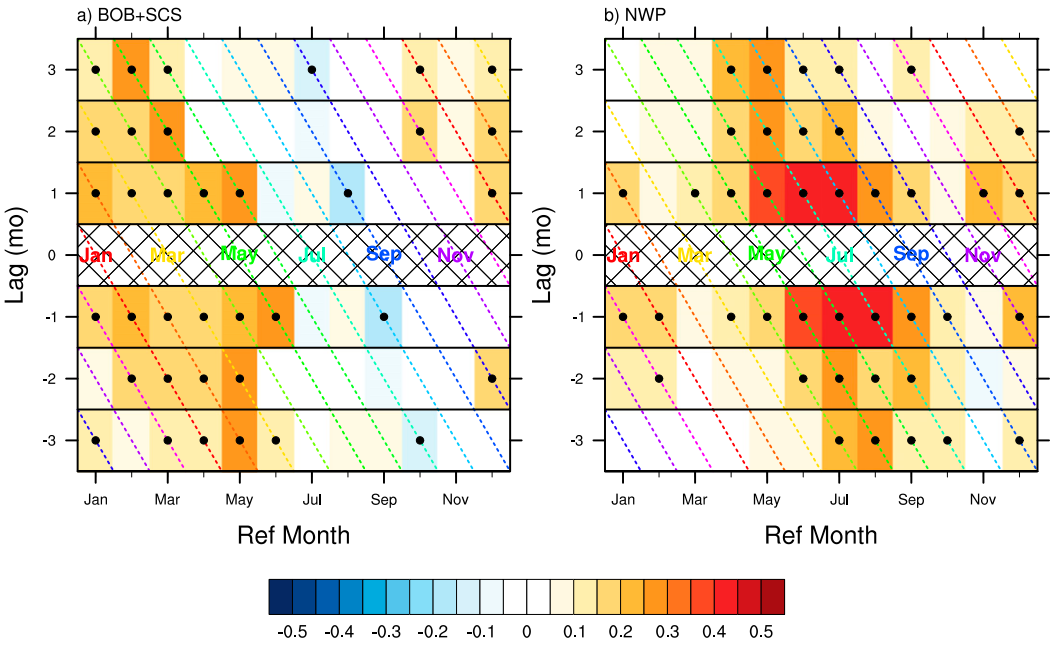

FIG. 9. Autocorrelation of SLP in (a) the BOB and SCS (5°–25°N, 80°–120°E) and (b) the NWP (10°–25°N, 120°–180°E) in cPOGA. Positive and negative numerals on the *Y* axis denote the lag in months after and before the reference month, respectively. Correlations above the 95% confidence levels, based on the *t* test, are stippled. Autocorrelations with zero lags are omitted.

Over the NWP, SLP shows strong persistence in summer (Fig. 9b). NWP SLP anomalies in May can persist through early summer but are not strongly correlated with preceding months. The NWP SLP in June and July shows high persistence and the autocorrelation is almost symmetrical between preceding and subsequent months. After August, the SLP correlation with subsequent months weakens but remains significant with preceding months. The evolution of the persistence pattern may be affected by both background SST and winds. During spring, the background SST is relatively cool over the tropical NWP north of 10°N (Fig. 10b), inhibiting the development of deep convection with a weaker local WES feedback than in other seasons. In the late summer and early fall, the easterly trades retreat eastward to 150°E (Fig. 10a). Local negative feedback prevents SLP anomalies from persisting in the mean westerly regime.

We have also examined the seasonal evolution of the coupling effect with two other metrics: the variance difference between the coupled and atmospheric POGA, and the pointwise correlation between local SST and precipitation in cPOGA (Fig. 10). As discussed above, the variance difference increases with positive ocean–atmosphere feedback. Local SST–precipitation correlation is commonly used to measure the ocean effect on the atmosphere (e.g., Trenberth and Shea 2005). Positive SST–precipitation correlation indicates the ocean as a driver for atmospheric variability, while weak or negative correlation may suggest that the ocean is passively influenced by and has weak feedback to the atmosphere (Wang et al. 2005; Wu and Kirtman 2007). Over the BOB and SCS, local SST–precipitation correlation is weak because of the cancellation between large-scale atmospheric variability (AAC) and the local SST effect on deep convection (Fig. 4d vs Fig. 6b). Over the NWP, the air–sea coupling intensifies the interannual variance of the SLP and precipitation but the SST–precipitation correlation is weak because of the nonlocal feedbacks from the NIO SST onto the AAC (see also Zhou et al. 2018).

6. Summary and discussion

We have studied the ENSO-free IPOC mode of regional Indo-NWP climate variability in ENSO-free models. By comparing a pair of atmospheric and coupled POGA experiments, we show that ocean–atmospheric interactions play an important role and this role varies with regions in summer. In the NWP, SLP shows large variance and enhanced persistence in the cPOGA as compared with aPOGA, but in the NIO the variance and persistence are reduced. The change in variance and persistence results from different types of ocean–atmosphere feedbacks.

We further examine the feedback processes by estimating the oceanic and atmospheric effects separately.

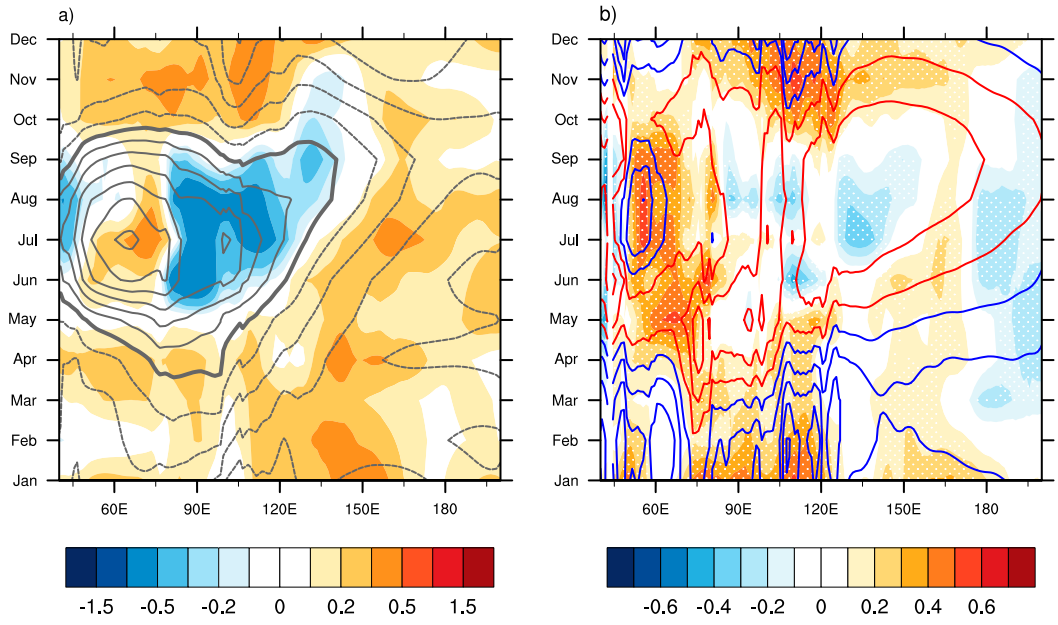

FIG. 10. (a) Fractional difference in interannual variance of monthly SLP between cPOGA and aPOGA [shading; (cPOGA − aPOGA)/cPOGA] and zonal background winds (contours every 2 m s^{-1}, with zero line thickened) averaged between 5° and 25°N in cPOGA. (b) Pointwise SST and precipitation correlation (shading with correlations >95% confidence level stippled, based on the *t* test) and climatological SST (contours, every 1 K; red contours denote SST ≥ 28°C) averaged between 5° and 25°N in cPOGA.

The SLP shows high interannual variability over the Indo-NWP region in summer. Anomalous high SLP over the NWP and NIO is accompanied with an AAC and suppressed precipitation. The atmospheric variability affects the ocean by inducing anomalous surface heat fluxes and ocean dynamical adjustments. Over the NWP where the northeasterly trades prevail, anomalous easterlies induced by local negative SST anomalies further cool the ocean by increasing evaporation, forming a positive feedback loop. Over the NIO, the anomalous easterlies of the AAC slow the background southwest monsoon wind, resulting in positive SST anomalies. The positive SST anomalies weakens the precipitation and SLP anomalies accompanied by the AAC as a negative feedback. Apart from the local feedback, the positive SST anomalies in the NIO help reinforce the NWP AAC via the Kelvin wave–induced divergence mechanism. This interbasin positive feedback, along with the positive WES feedback, explains why both the variance and persistence of SLP strengthen over the NWP in the coupled model compared to the atmospheric simulation.

Previous observational studies have shown that the NWP AAC affects the East Asia summer monsoon (Huang and Wu 1989; Chang et al. 2000) and the Indian summer monsoon (Chowdary et al. 2013, 2019; Zhou et al. 2019). Anomalous westerlies on the northwestern flank of the AAC can induce positive rainfall anomalies in the central China as a result of excessive moisture transport from the tropical oceans and orographic lift (Hu et al. 2017). A similar mechanism may also be applied to the ENSO-unrelated IPOC mode. Indeed, strong rainfall anomalies are found over East China and South Asia accompanied with the AAC without ENSO forcing (Figs. 4b,d). We suggest that the ocean–atmosphere coupling may enhance the predictability of Asian summer climate based on the enhanced persistence in the cPOGA. The NWP SST may serve as a potential predictor due to its lead correlation with the NWP AAC (Fig. 8c).

The summer NWP AAC may arise from the internal atmospheric variability without remote or local SST forcing (Zhou et al. 2018). Wang et al. (2020) very recently showed that the summer intraseasonal oscillation contributes importantly to month-to-month variability of the AAC as observed in the post–El Niño summer of 2016. Our study further shows that the coupled dynamics, largely determined by the background winds, can alter the spatial distribution and lifespan of the ENSO-unrelated IPOC mode. By definition, our focus on POGA ensemble spread excludes the ENSO influence but in reality, Indo–western Pacific variability is highly correlated with ENSO. In particular, the observed anomalies in post-ENSO summer closely resemble the free IPOC mode described in this study, including the interbasin coupling between NIO SST and the AAC over the NWP (e.g., Xie et al. 2009) as well as

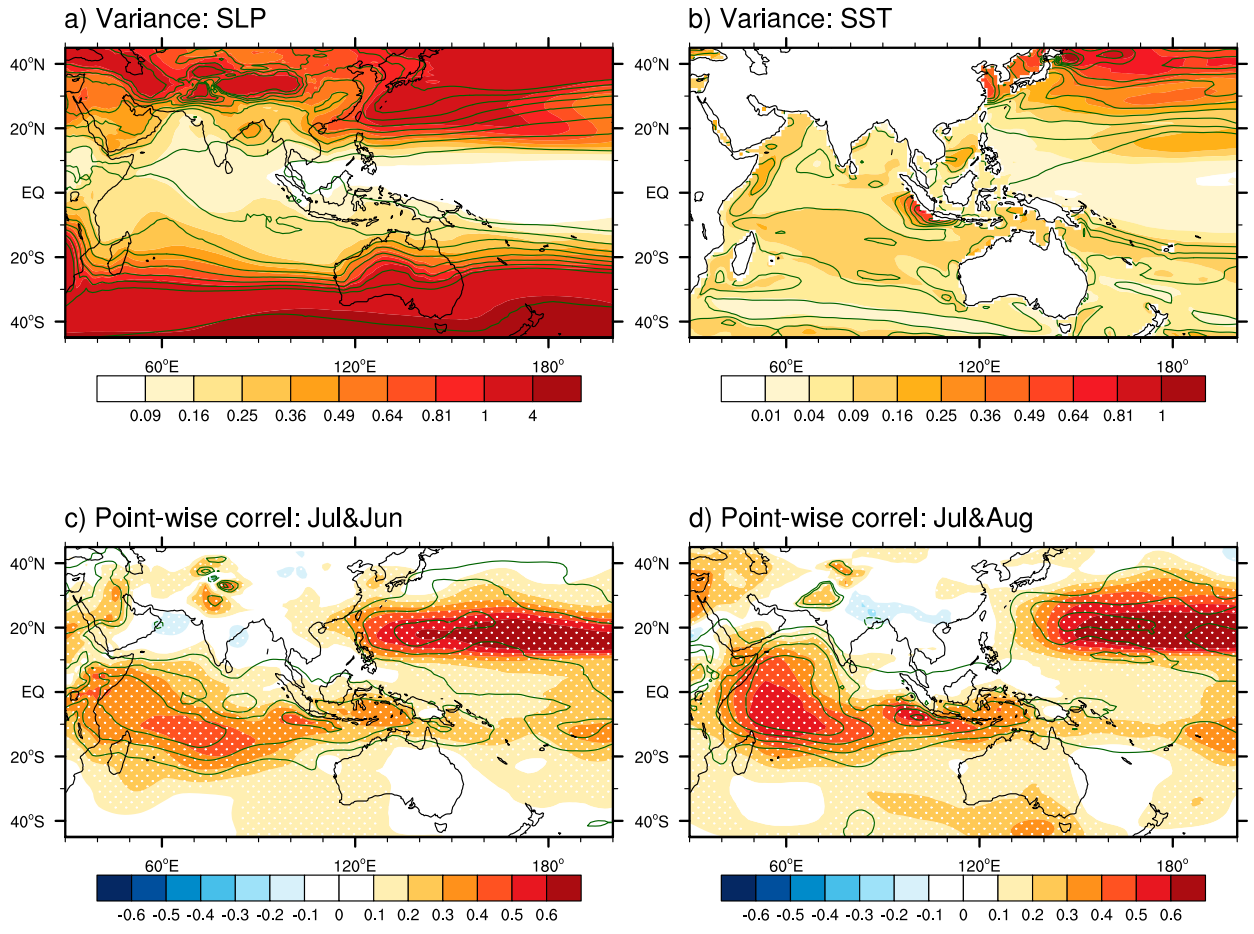

FIG. 11. Interannual variance of JJA (a) SLP (hPa^2) and (b) SST (K^2) in τ-NoENSO (shading) and cPOGA ensemble spread (contours). Also shown are pointwise correlations of (c) June and (d) August SLP with July SLP in τ-NoENSO (shading) and cPOGA ensemble spread (contours). Contour intervals are the same as the corresponding shading levels, with zero lines omitted.

the evolution from the preceding seasons (Wang et al. 2003). Due to the modulation by the seasonally varying background, El Niño induces a weak AAC over the NWP during the local cold seasons (Stuecker et al. 2015; Xie and Zhou 2017), triggering the IPOC mode that evolves through summer. As an additional trigger of IPOC, the El Niño forces the downwelling ocean Rossby waves and the resultant southwest IO warming that causes the southwesterly winds to weaken over the NIO (Du et al. 2009). Thus, the resemblance between the ENSO-unrelated IPOC and observed post-ENSO anomalies is not surprising. In fact, it is the positive coupled feedback that selects the IPOC mode as the most persistent and coherent pattern observed in post-ENSO summers.

In the cPOGA experiment, SST over the tropical eastern Pacific is restored to observations. This strong damping on ENSO-free, internal SST variability might propagate to the tropical IO through the weak temperature gradient approximation of the tropical troposphere. We have conducted a partial coupling experiment (τ-NoENSO) by overriding wind stress with the model climatology over the tropical Pacific (15°S–15°N, with a 5° buffer on the poleward boundaries). Like the cPOGA ensemble spread, there is no ENSO because of the lack of dynamical air–sea coupling in the tropical Pacific, but, unlike cPOGA, SSTs are allowed to evolve freely everywhere, including the tropical Pacific. Surface variability (including SST) over the Indo–western Pacific proves similar variance and persistence (Fig. 11) to that in the cPOGA ensemble spread. This suggests that atmospheric adjustments discussed here—specifically in wind and cloud—are more important than the weak temperature effect (Chiang and Sobel 2002) in propagating equatorial Pacific SST variability to the Indo–western Pacific warm pool.

Acknowledgments. We sincerely thank the three anonymous reviewers for the constructive comments and suggestions. This work is supported by the Natural

Science Foundation of China (41490640; 41490641), U.S. National Science Foundation (AGS 1637450), Japan Society for the Promoting Science (18H01278 and 19H05703), the Environment Research and Technology Development Fund (2-1904) of the Environmental Restoration and Conservation Agency of Japan, and the Japan Science and Technology Agency through Belmont Forum CRA "InterDec."

REFERENCES

Chang, C. P., Y. S. Zhang, and T. Li, 2000: Interannual and interdecadal variations of the East Asian summer monsoon and tropical Pacific SSTs. Part I: Roles of the subtropical ridge. *J. Climate*, **13**, 4310–4325, https://doi.org/10.1175/1520-0442(2000)013<4310:IAIVOT>2.0.CO;2.

Chiang, J. C., and A. H. Sobel, 2002: Tropical tropospheric temperature variations caused by ENSO and their influence on the remote tropical climate. *J. Climate*, **15**, 2616–2631, https://doi.org/10.1175/1520-0442(2002)015<2616:TTTVCB>2.0.CO;2.

Chowdary, J. S., C. Gnanaseelan, and S. Chakravorty, 2013: Impact of northwest Pacific anticyclone on the Indian summer monsoon region. *Theor. Appl. Climatol.*, **113**, 329–336, https://doi.org/10.1007/s00704-012-0785-9.

——, D. D. Patekar, G. Srinivas, C. Gnanaseelan, and A. Parekh, 2019: Impact of the Indo-western Pacific Ocean capacitor mode on South Asian summer monsoon rainfall. *Climate Dyn.*, **53**, 2327–2338, https://doi.org/10.1007/s00382-019-04850-w.

Delworth, T. L., and Coauthors, 2006: GFDL's CM2 global coupled climate models. Part I: Formulation and simulation characteristics. *J. Climate*, **19**, 643–674, https://doi.org/10.1175/JCLI3629.1.

Du, Y., S.-P. Xie, G. Huang, and K. Hu, 2009: Role of air–sea interaction in the long persistence of El Niño–induced North Indian Ocean warming. *J. Climate*, **22**, 2023–2038, https://doi.org/10.1175/2008JCLI2590.1.

Fan, L., S. I. Shin, Q. Liu, and Z. Liu, 2013: Relative importance of tropical SST anomalies in forcing East Asian summer monsoon circulation. *Geophys. Res. Lett.*, **40**, 2471–2477, https://doi.org/10.1002/grl.50494.

Frankignoul, C., and K. Hasselmann, 1977: Stochastic climate models, part II. Application to sea-surface temperature anomalies and thermocline variability. *Tellus*, **29**, 289–305, https://doi.org/10.3402/tellusa.v29i4.11362.

Gill, A. E., 1980: Some simple solutions for heat-induced tropical circulation. *Quart. J. Roy. Meteor. Soc.*, **106**, 447–462, https://doi.org/10.1002/qj.49710644905.

Hu, K., S.-P. Xie, and G. Huang, 2017: Orographically anchored El Niño effect on summer rainfall in central China. *J. Climate*, **30**, 10 037–10 045, https://doi.org/10.1175/JCLI-D-17-0312.1.

——, G. Huang, S.-P. Xie, and S. M. Long, 2019: Effect of the mean flow on the anomalous anticyclone over the Indo-northwest Pacific in post-El Niño summers. *Climate Dyn.*, **53**, 5725–5741, https://doi.org/10.1007/s00382-019-04893-z.

Huang, B., and Coauthors, 2015: Extended Reconstructed Sea Surface Temperature version 4 (ERSST.v4). Part I: Upgrades and intercomparisons. *J. Climate*, **28**, 911–930, https://doi.org/10.1175/JCLI-D-14-00006.1.

Huang, R. H., and Y. F. Wu, 1989: The influence of ENSO on the summer climate change in China and its mechanism. *Adv. Atmos. Sci.*, **6**, 21–32, https://doi.org/10.1007/BF02656915.

Izumo, T., C. B. Montégut, J.-J. Luo, S. K. Behera, S. Masson, and T. Yamagata, 2008: The role of the western Arabian Sea upwelling in Indian monsoon rainfall variability. *J. Climate*, **21**, 5603–5623, https://doi.org/10.1175/2008JCLI2158.1.

Kalnay, E., and Coauthors, 1996: The NCEP/NCAR 40-Year Reanalysis Project. *Bull. Amer. Meteor. Soc.*, **77**, 437–471, https://doi.org/10.1175/1520-0477(1996)077<0437:TNYRP>2.0.CO;2.

Kosaka, Y., and S.-P. Xie, 2013: Recent global-warming hiatus tied to equatorial Pacific surface cooling. *Nature*, **501**, 403–407, https://doi.org/10.1038/nature12534.

——, and ——, 2016: The tropical Pacific as a key pacemaker of the variable rates of global warming. *Nat. Geosci.*, **9**, 669–673, https://doi.org/10.1038/ngeo2770.

——, ——, N.-C. Lau, and G. A. Vecchi, 2013: Origin of seasonal predictability for summer climate over the northwestern Pacific. *Proc. Natl. Acad. Sci. USA*, **110**, 7574–7579, https://doi.org/10.1073/pnas.1215582110.

Lu, R., 2001: Interannual variability of the summertime North Pacific subtropical high and its relation to atmospheric convection over the warm pool. *J. Meteor. Soc. Japan*, **79**, 771–783, https://doi.org/10.2151/jmsj.79.771.

Ma, J., S.-P. Xie, and H. Xu, 2017: Intermember variability of the summer northwest Pacific subtropical anticyclone in the ensemble forecast. *J. Climate*, **30**, 3927–3941, https://doi.org/10.1175/JCLI-D-16-0638.1.

Matsuno, T., 1966: Quasi-geostrophic motions in the equatorial area. *J. Meteor. Soc. Japan*, **44**, 25–43, https://doi.org/10.2151/jmsj1965.44.1_25.

Ohba, M., and H. Ueda, 2006: A role of zonal gradient of SST between the Indian Ocean and the western Pacific in localized convection around the Philippines. *SOLA*, **2**, 176–179, https://doi.org/10.2151/SOLA.2006-045.

Rayner, N. A., D. E. Parker, E. B. Horton, C. K. Folland, L. V. Alexander, D. P. Rowell, E. C. Kent, and A. Kaplan, 2003: Global analyses of sea surface temperature, sea ice, and night marine air temperature since the late nineteenth century. *J. Geophys. Res.*, **108**, 4407, https://doi.org/10.1029/2002JD002670.

Stuecker, M. F., A. Timmermann, F.-F. Jin, S. McGregor, and H.-L. Ren, 2013: A combination mode of the annual cycle and the El Niño/Southern Oscillation. *Nat. Geosci.*, **6**, 540–544, https://doi.org/10.1038/ngeo1826.

——, F.-F. Jin, A. Timmermann, and S. McGregor, 2015: Combination mode dynamics of the anomalous northwest Pacific anticyclone. *J. Climate*, **28**, 1093–1111, https://doi.org/10.1175/JCLI-D-14-00225.1.

Sullivan, A., J.-J. Luo, A. C. Hirst, D. Bi, W. Cai, and J. He, 2016: Robust contribution of decadal anomalies to the frequency of central-Pacific El Niño. *Sci. Rep.*, **6**, 38540, https://doi.org/10.1038/srep38540.

Terao, T., and T. Kubota, 2005: East–west SST contrast over the tropical oceans and the post El Niño western North Pacific summer monsoon. *Geophys. Res. Lett.*, **32**, L15706, https://doi.org/10.1029/2005GL023010.

Trenberth, K. E., and D. J. Shea, 2005: Relationships between precipitation and surface temperature. *Geophys. Res. Lett.*, **32**, L14703, https://doi.org/10.1029/2005GL022760.

Wang, B., R. Wu, and X. Fu, 2000: Pacific–East Asian teleconnection: How does ENSO affect East Asian climate? *J. Climate*, **13**, 1517–1536, https://doi.org/10.1175/1520-0442(2000)013<1517:PEATHD>2.0.CO;2.

——, ——, and T. Li, 2003: Atmosphere–warm ocean interaction and its impacts on Asian–Australian monsoon variation.

J. Climate, **16**, 1195–1211, https://doi.org/10.1175/1520-0442(2003)16<1195:AOIAII>2.0.CO;2.

——, Q. Ding, X. Fu, I.-S. Kang, K. Jin, J. Shukla, and F. Doblas-Reyes, 2005: Fundamental challenge in simulation and prediction of summer monsoon rainfall. *Geophys. Res. Lett.*, **32**, L15711, https://doi.org/10.1029/2005GL022734.

Wang, C.-Y., S.-P. Xie, and Y. Kosaka, 2018: Indo-western Pacific climate variability: ENSO forcing and internal dynamics in a tropical Pacific pacemaker simulation. *J. Climate*, **31**, 10 123–10 139, https://doi.org/10.1175/JCLI-D-18-0203.1.

Wang, D. X., Q. Xie, Y. Du, W. Wang, and J. Chen, 2002: The 1997–1998 warm event in the South China Sea. *Chin. Sci. Bull.*, **47**, 1221–1227, https://doi.org/10.1007/BF02907614.

Wang, X., S. Xie, and Z. Guan, 2020: Atmospheric internal variability in the summer Indo–northwestern Pacific: Role of the intraseasonal oscillation. *J. Climate*, **33**, 3395–3410, https://doi.org/10.1175/JCLI-D-19-0794.1.

Wu, R., and B. P. Kirtman, 2007: Regimes of seasonal air–sea interaction and implications for performance of forced simulations. *Climate Dyn.*, **29**, 393–410, https://doi.org/10.1007/s00382-007-0246-9.

——, and S.-W. Yeh, 2010: A further study of the tropical Indian Ocean asymmetric mode in boreal spring. *J. Geophys. Res.*, **115**, D08101, https://doi.org/10.1029/2009JD012999.

——, B. P. Kirtman, and V. Krishnamurthy, 2008: An asymmetric mode of tropical Indian Ocean rainfall variability in boreal spring. *J. Geophys. Res.*, **113**, D05104, https://doi.org/10.1029/2007JD009316.

Xie, S.-P., and Z.-Q. Zhou, 2017: Seasonal modulations of El Niño–related atmospheric variability: Indo–western Pacific Ocean feedback. *J. Climate*, **30**, 3461–3472, https://doi.org/10.1175/JCLI-D-16-0713.1.

——, Q. Xie, D. X. Wang, and W. T. Liu, 2003: Summer upwelling in the South China Sea and its role in regional climate variations. *J. Geophys. Res.*, **108**, 3261, https://doi.org/10.1029/2003JC001867.

——, K. Hu, J. Hafner, H. Tokinaga, Y. Du, G. Huang, and T. Sampe, 2009: Indian Ocean capacitor effect on Indo–western Pacific climate during the summer following El Niño. *J. Climate*, **22**, 730–747, https://doi.org/10.1175/2008JCLI2544.1.

——, Y. Kosaka, Y. Du, K. Hu, J. Chowdary, and G. Huang, 2016: Indo-western Pacific Ocean capacitor and coherent climate anomalies in post-ENSO summer: A review. *Adv. Atmos. Sci.*, **33**, 411–432, https://doi.org/10.1007/s00376-015-5192-6.

Yang, Y., S.-P. Xie, L. Wu, Y. Kosaka, N.-C. Lau, and G. A. Vecchi, 2015: Seasonality and predictability of the Indian Ocean dipole mode: ENSO forcing and internal variability. *J. Climate*, **28**, 8021–8036, https://doi.org/10.1175/JCLI-D-15-0078.1.

Zhang, R. H., A. Sumi, and M. Kimoto, 1996: Impact of El Niño on the East Asian monsoon: A diagnostic study of the '86/87 and '91/92 events. *J. Meteor. Soc. Japan*, **74**, 49–62, https://doi.org/10.2151/jmsj1965.74.1_49.

Zhang, Y., S.-P. Xie, Y. Kosaka, and J. C. Yang, 2018: Pacific decadal oscillation: Tropical Pacific forcing versus internal variability. *J. Climate*, **31**, 8265–8279, https://doi.org/10.1175/JCLI-D-18-0164.1.

Zhou, Z.-Q., S.-P. Xie, G. J. Zhang, and W. Zhou, 2018: Evaluating AMIP skill in simulating interannual variability over the Indo–western Pacific. *J. Climate*, **31**, 2253–2265, https://doi.org/10.1175/JCLI-D-17-0123.1.

——, R. Zhang, and S.-P. Xie, 2019: Interannual variability of summer surface air temperature over central India: Implications for monsoon onset. *J. Climate*, **32**, 1693–1706, https://doi.org/10.1175/JCLI-D-18-0675.1.